Electronic transport and scattering times in tungsten-decorated graphene

Jamie A. Elias[1] and Erik A. Henriksen[1,2,*]

[1]*Department of Physics, Washington University in St. Louis, 1 Brookings Dr., St. Louis, Missouri 63130, USA*

[2]*Institute for Materials Science & Engineering, Washington University in St. Louis, 1 Brookings Dr., St. Louis, Missouri 63130, USA*

(Received 30 October 2016; revised manuscript received 2 January 2017; published 7 February 2017)

The electronic transport properties of a monolayer graphene device have been studied before and after the deposition of a dilute coating of tungsten adatoms on the surface. For coverages up to 2.5% of a monolayer, we find tungsten adatoms simultaneously donate electrons to graphene and reduce the carrier mobility, impacting the zero- and finite-field transport properties. Two independent transport analyses suggest the adatoms lie nearly 1 nm above the surface. The presence of adatoms is also seen to impact the low-field magnetoresistance, altering the signatures of weak localization.

DOI: 10.1103/PhysRevB.95.075405

I. INTRODUCTION

The two-dimensional electronic system in single layer graphene is inherently unprotected from external influences and thus can be readily altered by proximity to supporting substrates and incidental adsorbates [1–3]. A common and predictable outcome of such interactions is a more disordered electronic system. However there is also the potential to use surface adsorbates to advantageously alter the electronic properties of graphene; an example is the recent focus on boosting the weak native spin-orbit interaction in graphene in hopes of engineering topological band structure effects [4,5]. A key motivation for this pursuit is the possibility of realizing the Kane-Mele Hamiltonian [6], which consists of the relativistic Dirac-like dispersion of graphene plus an intrinsic spin-orbit coupling (SOC) term that together give rise to a quantum spin Hall insulator. To date, numerous theoretical works address the potential of several different transition metal atoms to play the role of spin-orbit donors leading to graphene-based topologically insulating systems [4,5,7–17]. Furthermore, there is a wide range of proposals for altering the electronic properties of graphene with adatoms beyond spin-orbit physics, including the possibility of novel magnetic systems [18,19] and even superconductors [20,21].

In this work we explore the effect of tungsten (W) adatoms on the electronic transport of single layer graphene. We find that dilute W coatings cause a significant charge doping along with an increase in scattering and reduced mobility. We experimentally investigate several characteristic scattering times via measurements of the zero-field conductivity, Shubnikov-de Haas oscillations of the magnetoresistance, and low-field signatures of weak localization (WL) in magnetoresistance. Our findings are consistent with a picture of isolated W adatoms that become ionized upon donating charge to the graphene, and hence increase the scattering potential experienced by the electrons.

II. EXPERIMENT

Electronic transport measurements were performed in a cryostat with a 13.5 T superconducting solenoid, using a custom-built sample stage in which graphene samples are mounted facing down toward a small thermal evaporator. Unless otherwise noted, all measurements were made at 4.3 K. Tungsten wires, 20 μm in diameter and of 99.95% purity, are located approximately 8 cm below the sample for use as evaporation sources. The evaporation rate of W atoms is controlled by passing a current through the wire while simultaneously monitoring any changes that occur in the electronic transport of the sample. During evaporation, the sample temperature rises to approximately 40 K while the rest of the cryostat remains close to 4 K. The density of adatoms that interact with the graphene may be estimated by the observed changes in charge doping as discussed below, and independently by measuring the change in diameter of the tungsten wire sources. Graphene samples are produced starting with mechanical exfoliation of Kish graphite onto Si wafers having a 300 nm thermal oxide, followed by fabrication of electrical contacts by electron beam lithography and thin film Cr/Au deposition. Transport data is acquired before and after evaporation using standard low-frequency AC lock-in techniques. Applying a gate voltage V_g to the degenerately doped Si substrate allows control of the free carrier density in graphene, $n = \alpha(V_g - V_{g0})$, where the coefficient $\alpha = 7.0 \times 10^{10}$ cm^{-2}V^{-1} is determined from oscillations in the magnetoresistance at high fields, and V_{g0} is the gate voltage for which the average carrier density is zero. Here we present results from a single layer graphene sample etched by an O_2 plasma into a 2-μm-wide Hall bar shown inset to Fig. 1(a); similar behavior has been observed in a second sample (see Supplemental Material [22]).

The deposition of tungsten atoms on to the surface of graphene impacts the electronic transport in several ways that will be presented below. Clearly an independent measurement of the deposited adatom density is desirable. Here we estimate this density by measuring the diameter of a tungsten wire source in a scanning electron microscope both before and after the experiment. Assuming the atoms are evaporated uniformly in all directions, geometry enables an estimate of the adatom density on the graphene. Two W wires were employed, with one used for the first two evaporations and another for the third evaporation. Adsorption of tungsten atoms results in electron doping of the graphene as will be discussed; however for now we simply note that the charge transfer due to the first two evaporations roughly equals that of the third. The W wire radius was reduced from 10.2 to 9.7μm (see Supplemental

*henriksen@wustl.edu

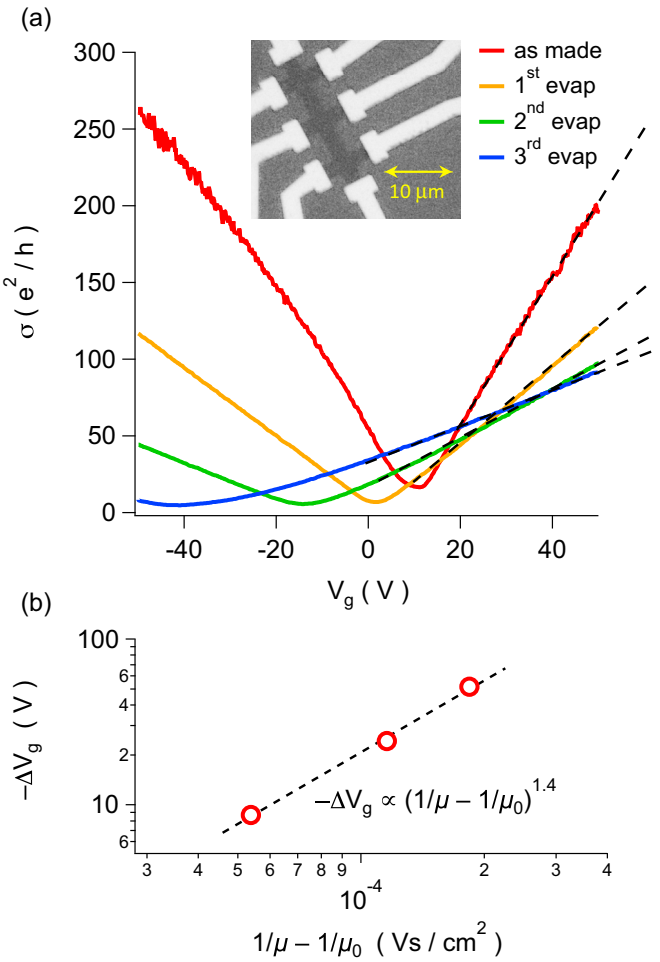

FIG. 1. (a) Conductivity σ vs gate voltage V_g for the monolayer graphene Hall bar sample shown inset to the figure. The as-made sample has a conductivity minimum at $V_{g0} = 10$ V, which shifts to the left indicating electron doping after each of three subsequent tungsten evaporations. Black dashed lines show linear fits used to extract the field-effect carrier mobility. (b) The gate voltage shift, $\Delta V_g = V_{g,\min} - V_{g0}$, with $V_{g,\min}$ the gate voltage position of the minimum conductivity in part (a) for each evaporation, plotted against the change in the inverse mobility, where μ_0 is the mobility of the as-made trace [red curve in part (a)]. The shift has a power law dependence on the inverse mobility with a slope of 1.4, consistent with pointlike scattering [3,26,29].

Material [22]), and we estimate that a 10-mm length of each wire was active in the evaporation. This yields a *total* deposited density after all three evaporations of $5 \pm 1 \times 10^{13}$ atoms/cm^2, covering 2.5% of the unit cells in graphene (or about 1 W atom per 80 C atoms).

III. RESULTS

A. Transport at zero magnetic field

Figure 1(a) shows the measured conductivity σ as a function of gate voltage for the sample used in this study, starting with data obtained from the as-made device (red trace) and continuing with traces recorded after three successive depositions of tungsten atoms, shown as the orange, green, and blue curves. With $n \propto V_g$, each trace exhibits a linear dependence on carrier density away from the conductivity minimum. This implies a constant carrier mobility, $\mu = (1/e)d\sigma/dn$, where e is the electron charge, that is observed to decrease after each evaporation. The initial mobility is 16 600 cm^2/Vs, falling to 8800, 5700, and finally 4100 cm^2/Vs with each successive evaporation. Moreover the charge neutrality point at the conductivity minimum of each curve is seen to shift to the left indicating electron doping of the graphene; and the curvature of the conductivity minimum broadens, suggesting an increase in carrier density inhomogeneity [23]. Broadly, these observations are consistent with prior works on the impact of potassium adatoms on graphene [3,24]; Ti, Fe, and Pt adatoms [25]; Au adatoms [26]; indium [23,27]; and iridium as well [28]; and altogether strongly suggest that W adatoms donate electrons to graphene, becoming ionized impurities that enhance the scattering and reduce the mobility.

Away from the minimum in conductivity at charge neutrality, the conductivity of graphene can be written as [29–31]

$$\sigma^{-1}(n) = \sigma_{ci}^{-1}(n) + \sigma_{sr}^{-1}, \tag{1}$$

reflecting two sources of scattering: screened charged impurities and short-ranged scattering as might arise at edges or vacancies. In the former case the conductivity is linear in the carrier density, $\sigma_{ci}(n) = C|n|/n_{\rm imp}$ where $n_{\rm imp}$ is the impurity density and C has been theoretically calculated [29] to be $C \approx 20e^2/h$ in the limit that the charged impurities lie in the graphene plane. Short-ranged impurities, on the other hand, lead to a conductivity that is independent of density. In many graphene-on-SiO_2 devices including those used in this work, $\sigma_{sr} \gg \sigma_{ci}$ and thus the conductivity is simply observed to be linear in density.

The conductivity data in Fig. 1(a) along with Eq. (1) allow us to extract (i) the added charge density $\Delta n = \alpha \Delta V_g$ donated by the adatoms, where ΔV_g is the shift of the conductivity minimum along the gate voltage axis due to charge doping; and (ii) the impurity density $n_{\rm imp} = (C/e)(1/\mu)$, which increases with each evaporation and includes a contribution $n_{\rm imp,0}$ from the initial (and uncontrolled) impurity distribution. The average height z of the adatoms above the graphene can also be extracted; the analysis is described below. We list all these values in Table I.

Naively, one might expect each adatom to donate one electron such that $\Delta n = \Delta n_{\rm imp} = n_{\rm imp} - n_{\rm imp,0}$. However, the data in Table I show an induced charge density that is 2 to 3 times larger than $\Delta n_{\rm imp}$. We note to determine $n_{\rm imp}$ we use the value $C = 20e^2/h$ which is strictly true only for $z = 0$, where z is the effective height of the impurities above the graphene plane. In fact, a self-consistent theory

TABLE I. Adatom-induced electron density Δn determined from the shift in minimum conductivity; the impurity density $n_{\rm imp} = (C/e)(1/\mu)$; and the height of impurities above the plane, z, in nm, calculated using the theory of Adam *et al.* as discussed in the text [29].

State of sample	Δn (cm^{-2})	$n_{\rm imp}$ (cm^{-2})	z (nm)
As made	0	2.9×10^{11}	0.08
1st evap.	6.1×10^{11}	5.5×10^{11}	0.6
2nd evap.	1.7×10^{12}	8.5×10^{11}	0.92
3rd evap.	3.6×10^{12}	1.2×10^{12}	1.1

of electronic transport dominated by charged impurity scattering by Adam *et al.* predicts [29] that C both increases and has a superlinear density dependence for $z > 0$, e.g., $C(z = 1) \approx 30$. Additionally, since density functional theory (DFT) calculations predict that W atoms should donate between 0.56 and 0.93 electrons/atom [32,33], we believe the 2 to 3 electrons/atom implied by Table I is an erroneous result of using $z = 0$. Therefore we continue by first *assuming* $\Delta n = \Delta n_{\rm imp}$, and then determining the value of z needed to make the theoretically calculated conductivity match the data. The fact that C increases with z explains why $n_{\rm imp}$ is initially underestimated. Pursuing this calculation, for increasing W coverage we find z grows to just over 1 nm. This is rather larger than the $z = 0.16$ to 0.17 nm separation predicted for W atoms above the center of a graphene honeycomb by DFT calculations [13,34]; however, z is an effective height parameter accounting for the distance of one charged impurity from a perfect two-dimensional (2D) plane, which is certainly an oversimplification. We note that using the DFT-predicted charge transfer values would increase z by roughly 30%.

In Fig. 1(b) we plot the shift in gate voltage $-\Delta V_g$ vs the change in the inverse mobility, $1/\mu - 1/\mu_0$. This quantity is both predicted and experimentally found to obey a power law, $-\Delta V_g \propto (1/\mu - 1/\mu_0)^b$, where b is typically 1.2 to 1.3 for pointlike charged impurities (as opposed to clusters, for which $b < 1$) [3,26,29]. Here we find $b = 1.4$. Altogether this zero-field conductivity analysis implies that W adatoms are isolated, charged impurities lying approximately 1 nm above the surface.

B. Comparison of transport and quantum scattering times

We now investigate the behavior of the transport and quantum scattering times, τ_μ and τ_q, as W atoms are deposited on graphene. Both parameters are a measure of electron scattering, but where the single particle relaxation (or "quantum") time τ_q is sensitive to *all* scattering events, the transport time τ_μ only measures those that contribute to the resistance of the material, e.g., forward scattering processes are ignored. In standard 2D systems, backscattering (where $|\mathbf{k}_{\rm final} - \mathbf{k}_{\rm initial}| = 2k_F$) is the most efficient at limiting τ_μ, but these events are suppressed in single layer graphene [38] leaving "right-angle" scattering to have the strongest impact on the transport time. The scattering rates are found by integrating over the total angular scattering potential $Q(\theta)$ as

$$\frac{1}{\tau_q} = \int_0^\pi Q(\theta)(1 + \cos\theta)d\theta,$$
$$\frac{1}{\tau_\mu} = \int_0^\pi Q(\theta)(1 - \cos^2\theta)d\theta,$$

where factors of $1 + \cos\theta$ in each formula account for the suppression of $2k_F$ scattering, and the additional factor of $1 - \cos\theta$ in the transport scattering rate accounts for the limited impact of forward scattering.

The ratio τ_μ/τ_q can be used to discriminate between the type and location of scattering potentials. For instance short-range (δ function) impurities scatter equally into all angles and thus $\tau_\mu = 2\tau_q$, where the factor of 2 is linked to the absence of backscattering. Meanwhile Coulomb scattering leads to an increase in forward scattering events due to its long-ranged nature [37,39], so that $\tau_\mu/\tau_q > 2$. Indeed in high mobility GaAs 2D systems, τ_μ/τ_q can exceed 100 due to the exceptional purity of the host crystal and the fact that ionized impurities are removed many tens of nm from the 2D layer.

In graphene-on-SiO_2 this ratio is generally expected to be small due to strong scattering caused by close coupling of the graphene sheet to the substrate, as indeed was observed by Hong *et al.* [36] and Monteverde *et al.* [40]. The basic theoretical picture predicts that $\tau_\mu/\tau_q < 2$ for short-ranged scattering (such as vacancies [41]), and $\tau_\mu/\tau_q > 2$ for (screened) Coulomb scattering [37]. For charged impurities that lie a distance z above the plane the ratio becomes increasingly larger, since more distant Coulomb scatterers yield smaller scattering angles, preferentially limiting the quantum scattering time. The ratio can also depend on whether impurities are either isolated or clumped together in clusters; in the latter case the charge doping efficiency and hence the number of ionized scatterers is reduced [26]. Indeed, for clusters the ratio τ_μ/τ_q is predicted to increase by roughly the number of impurities per cluster as the total scattering cross section outstrips the rate of backscattering [42]. From the experimental references just cited, it is apparent that transport in different batches of graphene-on-SiO_2 samples can yield a range of ratios implying the dominance of either Coulomb [36] or short-range [40] scattering.

To learn more about the impact of W adatoms, we have studied the τ_μ/τ_q ratio in our sample as it is impacted by tungsten adatoms. We extract the transport scattering time from the conductivity data of Fig. 1 using the relation $\sigma = (2e^2/h)\sqrt{\pi n}v_F\tau_\mu$, where v_F is the Fermi velocity, and the τ_q values from an analysis of Shubnikov-de Haas (SdH) oscillations of the magnetoresistance at high magnetic fields and over a range of carrier densities for electron-doped graphene, in the as-made sample and following each evaporation. The amplitude of Shubnikov-de Haas oscillations is generally well described by the first term of the Lifshitz-Kosevich equation [43],

$$\frac{\delta\rho_{xx}}{\rho_0} = 4X_{th}\exp\left(-\frac{\pi}{\omega_c\tau_q}\right);\ X_{th} = \frac{2\pi^2 k_B T/\hbar\omega_c}{\sinh(2\pi^2 k_B T/\hbar\omega_c)},$$

where $\rho_0 = \rho(B = 0)$ and $\omega_c = eB/m^*$ is the cyclotron frequency with the effective mass $m^* = \hbar\sqrt{\pi n}/v_F$.

Figure 2(a) shows a representative SdH trace at a density $n = 4.3 \times 10^{12}$ cm^{-2} after the second tungsten evaporation. The logarithm of the amplitude of the oscillations, divided by ρ_0 and the thermal damping factor X_{th}, yields a straight line when plotted vs $1/B$ as shown in Fig. 2(b), with a slope that is inversely proportional to the quantum scattering time [35,36]. The transport and quantum scattering times we find are plotted in Fig. 2(c) and 2(d), respectively. Both follow a roughly $\sqrt{n}$ dependence, shown by the dashed red curves.

In Fig. 2(e) we plot the ratio of these scattering times as a function of carrier density, for the as-made sample and following each evaporation. A clear downward trend is visible with the ratio dropping from 6 to 7 down to 3 to 4 over the course of the depositions. While the ratio is more or less constant in the as-made sample, with each evaporation a slight but clear increase in the slope emerges. The density

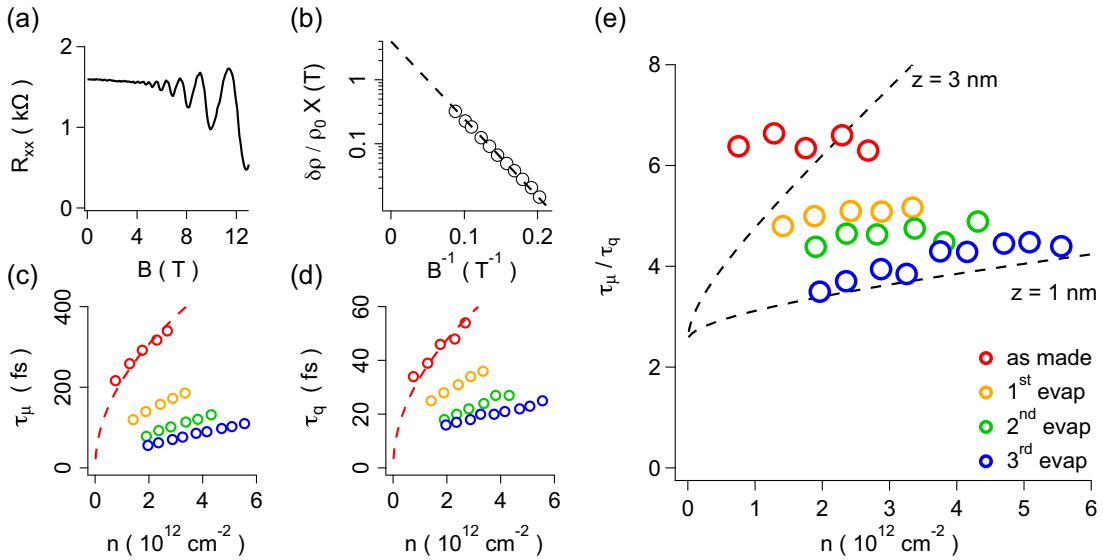

FIG. 2. (a) Representative Shubnikov-de Haas trace after the second W evaporation, at a density $n = 4.3 \times 10^{12}$ cm^{-2}. (b) The corresponding analysis of the temperature-corrected oscillation amplitudes vs B^{-1} after Coleridge [35] and Hong [36]; the linear fit is constrained to a y intercept of 4, and the slope is proportional to the quantum scattering rate τ_q^{-1}. (c),(d) Transport and quantum scattering times extracted from conductivity data of Fig. 1 and analysis of SdH traces, respectively. Red dashed lines are $\sqrt{n}$ fits to red circles. (e) Ratio of transport to quantum scattering time, τ_μ/τ_q, vs carrier density n for the as-made sample and after each evaporation. Uncertainty in the data is given by the symbol size. The dashed black lines are calculated using the theory of Hwang and Das Sarma [37], for the case of pure charged impurity scattering.

range explored is limited by a combination of the shift in the minimum conductivity due to electron doping, and the associated decrease in mobility which smears out SdH oscillations at lower densities. We compare these data to two curves calculated using the theory of Hwang and Das Sarma [37] that illustrate the predicted variation of τ_μ/τ_q for the case of pure charged impurity scattering, where the effective height z above the graphene sheet is chosen to be either $z = 1$ or $z = 3$ nm. The impurity potential in the as-made sample is uncontrolled and likely reflects a range of sources including both charged and short-ranged impurity scattering; thus the rather poor agreement with the "3 nm" curve is not surprising. However upon successive adatom depositions, the ratio falls lower to show good agreement with the "1 nm" curve. This is consistent with a picture where W adatoms constitute charged impurities close to the graphene, which comes to dominate the built-in impurity potential. This value for the adatom-graphene separation agrees with that found from a consideration of the zero-field conductivity, although in both cases the height enters each theory as an exponential in the scattering rate integral, so this agreement is not wholly unexpected. As previously noted, however, the separation distance for tungsten adatoms predicted by DFT calculations is rather smaller, $z = 0.16$ to 0.17 nm [13,34]. A similar discrepancy in separation distances was found for indium adatoms [23].

Finally we note that although the final impurity-graphene separation of 1 nm found from the scattering time ratio agrees with the zero-field conductivity analysis above, the *initial* separations prior to any W deposition are in sharp disagreement. This probably speaks to our ignorance of the impurity distribution in the as-made sample, in which scattering sources other than charged impurities will play a larger role. For instance, we have not isolated the contribution of long- and short-ranged scattering in our analysis of the zero-field conductivity; as in all cases the linear-in-n scattering dominates and obscures the contribution of density-independent scattering. Yet, the theories we are comparing to here account only for charged impurity scattering, and so may not describe the as-made sample very well.

C. Weak localization

At magnetic fields below 50 mT, the sample shows clear signs of WL in the magnetoresistance. Figure 3 shows four traces, plotted as $\delta\rho/\rho_0^2$ where $\delta\rho = \rho(B) - \rho_0$, for the as-made sample and following each evaporation at a carrier density of $n = 1.4 \times 10^{12}$ cm^{-2}. All four traces show a narrow peak that is roughly e^2/h in magnitude, along with universal conductance fluctuations that are symmetric in the field. With each evaporation both the localization peak and the conductance fluctuation features are seen to broaden and become reduced in amplitude.

Analysis of the localization correction to the conductivity can yield useful information on characteristic scattering times including the phase coherence time τ_ϕ and various other scattering mechanisms [44]. In graphene these may include intervalley scattering rates, intravalley scattering processes including sublattice symmetry effects and trigonal warping of the Dirac cones, and spin-orbit effects [45–47]. We perform fits to our data using a simplified version of the theory developed by McCann & Fal'ko *et al.* which ignores small corrections to the WL due to intravalley scattering processes [48]:

$$\frac{\Delta\rho}{\rho_0^2} = -\frac{e^2}{\pi h}\left[F\left(\frac{B}{B_\phi}\right) - F\left(\frac{B}{B_\phi + 2B_i}\right)\right],$$
$$F(z) = \ln(z) + \psi\left(\frac{1}{2} + \frac{1}{z}\right), \quad B_{\phi,i} = \frac{\hbar}{4De}\tau_{\phi,i}^{-1}. \qquad (2)$$

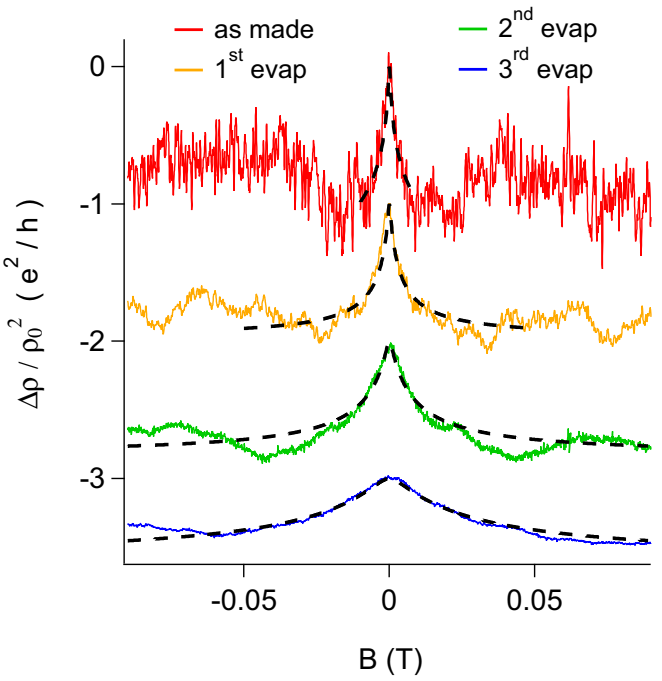

FIG. 3. Low-field magnetoresistance for a carrier density $n = 1.4 \times 10^{12}$ cm^{-2}, showing characteristic WL peaks about $B = 0$. Traces are vertically offset for clarity. The dashed black lines are fits using Eq. (2), with the field range restricted to the diffusive regime $(l_\mu/l_B)^2 \ll 1$; the fitting parameters are plotted in Fig. 4.

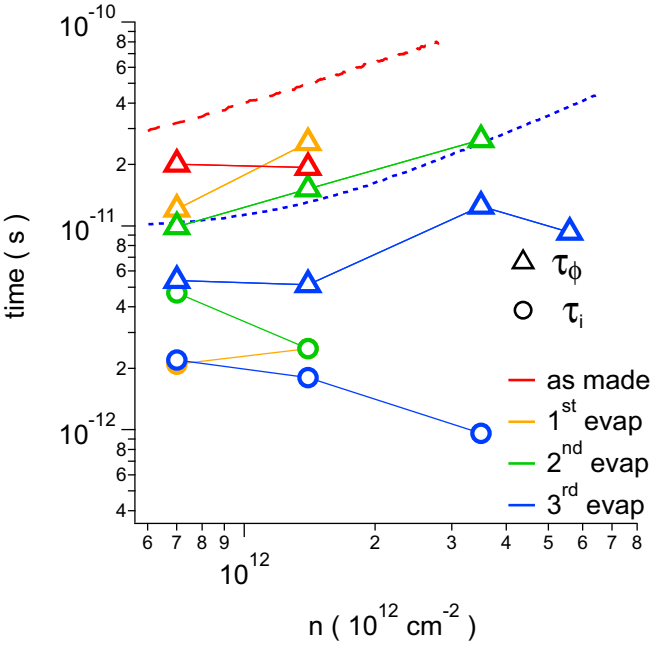

FIG. 4. Phase-breaking time τ_ϕ and intervalley scattering time τ_i extracted from curve fits to the low-field magnetoresistance using Eq. (2), as illustrated in Fig. 3. The theoretical phase breaking times calculated with Eq. (3) are shown as lines in the upper portion of the figure, using data from the as-made sample (dashed red) and after the 3rd evaporation (dotted blue). Trends in the data reflect the increase (decrease) in conductivity with carrier density (successive evaporations).

Here $D = v_F^2\tau_\mu/2$ is the diffusivity and ψ is the digamma function. Use of this simplified theory is justified by the fact that graphene-on-SiO_2 samples typically have a high intravalley scattering rate that results in a negligible contribution to localization effects [48–50]. Indeed in comparing fits to our data made using either Eq. (2) or the full WL expression for graphene [45], we find virtually no difference in the fitting curves; however, the inclusion of a third fitting parameter for intravalley scattering in the full theory leads to χ^2 values that are poorly constrained, with large uncertainties in the scattering times. Thus we use this two-parameter fit to obtain numerical estimates of τ_ϕ and τ_i, over a B field range such that the elastic mean free path (here, taken as equal to $l_\mu = v_F\tau_\mu$) is much less than the magnetic length [51], $l_{el}^2 \ll l_B^2$, where $l_B = \sqrt{\hbar/eB}$.

Figure 4 shows the values of the dephasing time τ_ϕ and the intervalley scattering time τ_i from our fitting procedure. The differing density ranges used for the as-made sample and each separate evaporation are a consequence of the electron doping which, for the fixed gate voltage range employed in this sample, accesses a greater span of electron densities with each successive deposition. Not shown in Fig. 4 is the distribution of transport scattering times, but even the largest τ_μ measured—in the as-made sample at the highest density explored—is only 0.3 ps so that in all cases τ_i exceeds τ_μ by one or two orders of magnitude. Generally speaking, we find the dephasing times τ_ϕ show a modest increase with carrier density and a decrease with each tungsten deposition. Such behavior is in accordance with the predictions of Altshuler *et al.* [52]:

$$\tau_\phi^{-1} = \frac{k_B T}{2\hbar}\frac{\ln(\pi\hbar\nu D)}{\pi\hbar\nu D} = \frac{k_B T}{2\hbar}\frac{\ln(k_F l)}{k_F l}, \tag{3}$$

with D again the diffusivity and ν the density of states at the Fermi level. The expression on the right includes the single layer graphene density of states $\nu = 2E_F/(\pi\hbar^2 v_F^2)$. This formula is plotted in Fig. 4 using the transport parameters for the as-made sample (red dashed line) and after the final tungsten evaporation (blue dotted line). The data follow the general trend illustrated by these curves, but lie a factor of 2 to 4 lower. This may indicate the presence of additional dephasing mechanisms such as flexural phonons [53], spin-orbit coupling (SOC) [47], or spin-flip scattering [54,55]. The latter, at least, seems unlikely: spin-flip scattering in graphene due to isolated fluorine adatoms yields phase-breaking lengths $l_\phi = \sqrt{D\tau_\phi} = 70$ to 200 nm at 4 K [54], compared to the $l_\phi = 300$ to 700 nm found here, despite the fluorine density being an order of magnitude lower than the W adatoms.

Tungsten atoms have a strong inherent SOC which has been predicted to be inherited by graphene [13]. Thus arguably we should study the low-field magnetoresistance with curve fits to the theory that incorporates the physics of spin-orbit scattering [47]. We have attempted this and find the fits to be generally inferior to those found using Eq. (2); for further discussion see the Supplemental Material [22]. Moreover, no obvious signatures of SOC, e.g., weak anti-localization [47,56,57], are observed. Altogether these findings suggest that scattering due

to an inherited spin-orbit interaction, if present at all, is very weak.

Meanwhile the values of τ_i, although suffering from a fair degree of scatter, do show a decreasing trend with each evaporation. This is surprising: since the charged tungsten adatoms presumably act as intravalley scatterers, an increase in τ_i is expected. This is due to the corresponding reduction of the diffusivity, which limits the time charge carriers spend near the sample edge where strong intervalley scattering is expected; a similar effect was observed for indium adatoms [23]. Here the intervalley times $\tau_i \approx 1$ to 5 ps correspond to scattering lengths $l_i = \sqrt{D\tau_i} = 200$ to 300 nm, rather smaller than the 2 μm width of the device.

IV. DISCUSSION

In this work we present the results of electronic transport measurements on a monolayer graphene device with an increasing, but always small, density of tungsten adatoms. Measurements of the zero-field conductivity, the ratio of transport and quantum scattering times, and WL in the magnetoresistance point toward a now-familiar picture [3,23–28] for metal adatoms wherein isolated impurities donate charge to the graphene substrate and become ionized impurities with a concomitant increase in scattering and reduction of the mobility. However there is one standout feature in our experiment, namely, as mentioned above we estimate that over 10 times as many W atoms were deposited as can be accounted for by the magnitude of electron doping measured by the shift in the minimum conductivity, under the assumption that each atom donates one electron. Relaxing this assumption to within the range of theoretically predicted values of 0.56 to 0.93 electrons/atom [32,33] does little to improve the match.

Regarding the W deposition, two scenarios immediately suggest themselves: first, the adatoms may form clusters, or second, fabrication residues may prevent many atoms from reaching the surface. In the former case, we note the migration energy for W adatoms (the difference between binding energies at three high-symmetric sites: atop a C atom, astride a C-C bond, or in the middle of a hexagon) is calculated [32] by DFT to be $E_m = 1.2$ eV. The hopping rate for migrating adatoms is given by [58] $R = (k_B T/h)\exp(-eE_m/k_B T)$, which for all practical purposes vanishes below 150 K for W atoms. For completeness we note this strongly disagrees with a separate DFT study [33] that finds the diffusion energy to be a mere 20 meV with the stable site at the "bridge" of the C-C bond; clearly this would change our expectations. In any event, these considerations apply to atoms already on the surface. However adatoms with a high kinetic energy freshly evaporated from the hot W wire may diffuse on the graphene surface before losing their energy via thermal radiation or phonon emission, and thus have the opportunity to form clusters. Clusters of metal atoms on graphene are known to be far less efficient at charge doping [26,28] and consequently have a limited impact on the mobility. However, the total scattering cross-section remains large for clusters; and indeed a key prediction [42] of cluster-dominated transport is a ratio τ_μ/τ_q that increases with increasing cluster size (and thus W dose), precisely the opposite of the observed relation.

Thus we consider a second possibility: that fabrication residues prevent most of the evaporated atoms from reaching the surface. The surface of graphene after standard fabrication procedures employing PMMA (polymethyl-methacrylate) as a resist for electron-beam lithography has been directly imaged by transmission electron microscopy [59,60], and a thin (∼nm) coating of PMMA molecules is found to remain even after aggressive thermal annealing procedures (which were not performed on our sample). These images reveal that a significant portion of the surface may be covered by this remnant PMMA, enough to perhaps account for the discrepancy between the expected density of W atoms based on the change in the source wire diameter, and the density inferred by the change in charge doping. This PMMA layer also provides a natural means to prevent clustering: if any hot tungsten atom does migrate upon landing, it will shortly encounter this impurity layer and come to a halt.

Density function theory calculations predict that W adatoms should induce a SOC into graphene [13], but we have not found any evidence in favor of this. The adatom density in our devices may be too low to generate a significant coupling, as the DFT calculations employed densities of $\approx 10^{14}$ cm^{-2}, a factor of 30 greater than the adatom density inferred by the change in charge doping. Alternatively, the induced SOC depends on just where the adatoms reside relative to the C atoms of the graphene lattice [5]. Thus the W adatoms may not be ideally located, or, given the large z values, are perhaps too far away.

V. CONCLUSION

In conclusion, we have performed a transport study of graphene with a dilute coating of W adatoms. The adatoms induce an electron doping of the graphene and a reduction of the mobility, enforcing a linear dependence of the conductivity on density consistent with charged impurity scattering. Analysis of the changes in the conductivity suggest the W atoms reside approximately 1 nm above the surface. Similar to the case of indium adatoms [23], this distance is unexpectedly large given that the atoms clearly are close enough to donate charge, and it also disagrees with the results of DFT calculations. One possibility is the height discussed in the self-consistent theory should be considered an "effective" distance that is correlated with, if not identical to, the actual physical separation that DFT attempts to calculate. This clearly requires further experimental investigation, preferably by a scanned probe method that is sensitive to the adatom height.

We have also performed a study of the ratio of the transport to quantum scattering time, τ_μ/τ_q, finding the ratio to decrease from 6 to 7 down to 3 to 4 as the density of W adatoms increases. The adatom height inferred by comparison to theoretical calculations is approximately 1 nm, in agreement with the estimate found from the zero-field conductivity.

Clear signatures of WL are seen at low magnetic fields. The dephasing times extracted from fits are in agreement with values expected from theory; however, no evidence for a SOC effect induced by proximity to W atoms is found, and we speculate the adatom density is too low for

a significant effect to be seen. The intervalley scattering times are shorter than expected, but the precise scattering potential of the as-made device is not known, and there may be defects or surface impurities that cause scattering with large momentum transfers. All transport data point to a picture wherein W deposition at low coverages leads to isolated charged impurities.

ACKNOWLEDGMENTS

We thank S. Adam, J. Alicea, U. Chandni, S. Das Sarma, M. Franz, M. Fuhrer, X. Hong, M. Lundeberg, R. Mong, J. Pollanen, and M.-F. Tu for helpful correspondence and discussions. The authors acknowledge support from Washington University and the Institute for Materials Science & Engineering, for the use and availability of IMSE instruments and staff.

[1] F. Schedin, A. Geim, S. Morozov, E. Hill, P. Blake, M. I. Katsnelson, and K. S. Novoselov, Nat. Mater. **6**, 652 (2007).
[2] C. Jang, S. Adam, J.-H. Chen, E. D. Williams, S. Das Sarma, and M. S. Fuhrer, Phys. Rev. Lett. **101**, 146805 (2008).
[3] J.-H. Chen, C. Jang, S. Adam, M. Fuhrer, E. D. Williams, and M. Ishigami, Nat. Phys. **4**, 377 (2008).
[4] C. Weeks, J. Hu, J. Alicea, M. Franz, and R. Wu, Phys. Rev. X **1**, 021001 (2011).
[5] J. Hu, J. Alicea, R. Wu, and M. Franz, Phys. Rev. Lett. **109**, 266801 (2012).
[6] C. L. Kane and E. J. Mele, Phys. Rev. Lett. **95**, 226801 (2005).
[7] A. H. Castro Neto and F. Guinea, Phys. Rev. Lett. **103**, 026804 (2009).
[8] K. H. Ding, Z. G. Zhu, and J. Berakdar, Europhys. Lett. **88**, 58001 (2009).
[9] Z. Qiao, S. A. Yang, W. Feng, W.-K. Tse, J. Ding, Y. Yao, J. Wang, and Q. Niu, Phys. Rev. B **82**, 161414 (2010).
[10] S. Abdelouahed, A. Ernst, J. Henk, I. V. Maznichenko, and I. Mertig, Phys. Rev. B **82**, 125424 (2010).
[11] J. Ding, Z. Qiao, W. Feng, Y. Yao, and Q. Niu, Phys. Rev. B **84**, 195444 (2011).
[12] H. Jiang, Z. Qiao, H. Liu, J. Shi, and Q. Niu, Phys. Rev. Lett. **109**, 116803 (2012).
[13] H. Zhang, C. Lazo, S. Blügel, S. Heinze, and Y. Mokrousov, Phys. Rev. Lett. **108**, 056802 (2012).
[14] O. Shevtsov, P. Carmier, C. Groth, X. Waintal, and D. Carpentier, Phys. Rev. B **85**, 245441 (2012).
[15] D. Ma, Z. Li, and Z. Yang, Carbon **50**, 297 (2012).
[16] P.-H. Chang, M. S. Bahramy, N. Nagaosa, and B. K. Nikolić, Nano Lett. **14**, 3779 (2014).
[17] J. Hu, Z. Zhu, and R. Wu, Nano Lett. **15**, 2074 (2015).
[18] H. Sevinçli, M. Topsakal, E. Durgun, and S. Ciraci, Phys. Rev. B **77**, 195434 (2008).
[19] T. Eelbo, M. Waśniowska, P. Thakur, M. Gyamfi, B. Sachs, T. O. Wehling, S. Forti, U. Starke, C. Tieg, A. I. Lichtenstein, and R. Wiesendanger, Phys. Rev. Lett. **110**, 136804 (2013).
[20] G. Profeta, M. Calandra, and F. Mauri, Nat. Phys. **8**, 131 (2012).
[21] B. M. Ludbrook, G. Levy, P. Nigge, M. Zonno, M. Schneider, D. J. Dvorak, C. N. Veenstra, S. Zhdanovich, D. Wong, P. Dosanjh, C. Straßer, A. Stöhr, S. Forti, C. R. Ast, U. Starke, and A. Damascelli, Proc. Natl. Acad. Sci. USA **112**, 11795 (2015).
[22] See Supplemental Material at http://link.aps.org/supplemental/10.1103/PhysRevB.95.075405 for the details of adatom density calculations, WL fitting functions, and similar results from a second sample.
[23] U. Chandni, E. A. Henriksen, and J. P. Eisenstein, Phys. Rev. B **91**, 245402 (2015).
[24] J. Yan and M. S. Fuhrer, Phys. Rev. Lett. **107**, 206601 (2011).
[25] K. Pi, K. M. McCreary, W. Bao, W. Han, Y. F. Chiang, Y. Li, S.-W. Tsai, C. N. Lau, and R. K. Kawakami, Phys. Rev. B **80**, 075406 (2009).
[26] K. M. McCreary, K. Pi, A. G. Swartz, W. Han, W. Bao, C. N. Lau, F. Guinea, M. I. Katsnelson, and R. K. Kawakami, Phys. Rev. B **81**, 115453 (2010).
[27] Z. Jia, B. Yan, J. Niu, Q. Han, R. Zhu, D. Yu, and X. Wu, Phys. Rev. B **91**, 085411 (2015).
[28] Y. Wang, S. Xiao, X. Cai, W. Bao, J. Reutt-Robey, and M. S. Fuhrer, Sci. Rep. **5**, 15764 (2015).
[29] S. Adam, E. H. Hwang, V. M. Galitski, and S. Das Sarma, Proc. Natl. Acad. Sci. USA **104**, 18392 (2007).
[30] K. Nomura and A. H. MacDonald, Phys. Rev. Lett. **96**, 256602 (2006).
[31] T. Ando, J. Phys. Soc. Jpn. **75**, 074716 (2006).
[32] K. Nakada and A. Ishii, in *Graphene Simulation*, edited by J. R. Gong (InTechOpen, Rijeka, Croatia, 2011), pp. 1–20.
[33] M. Manadé, F. Viñes, and F. Illas, Carbon **95**, 525 (2015).
[34] K. Nakada and A. Ishii, Solid State Commun. **151**, 13 (2011).
[35] P. T. Coleridge, Phys. Rev. B **44**, 3793 (1991).
[36] X. Hong, K. Zou, and J. Zhu, Phys. Rev. B **80**, 241415 (2009).
[37] E. H. Hwang and S. Das Sarma, Phys. Rev. B **77**, 195412 (2008).
[38] T. Ando, T. Nakanishi, and R. Saito, J. Phys. Soc. Jpn. **67**, 2857 (1998).
[39] S. Das Sarma and F. Stern, Phys. Rev. B **32**, 8442 (1985).
[40] M. Monteverde, C. Ojeda-Aristizabal, R. Weil, K. Bennaceur, M. Ferrier, S. Guéron, C. Glattli, H. Bouchiat, J.-N. Fuchs, and D. L. Maslov, Phys. Rev. Lett. **104**, 126801 (2010).
[41] T. Stauber, N. M. R. Peres, and F. Guinea, Phys. Rev. B **76**, 205423 (2007).
[42] M. I. Katsnelson, F. Guinea, and A. K. Geim, Phys. Rev. B **79**, 195426 (2009).
[43] V. P. Gusynin and S. G. Sharapov, Phys. Rev. B **71**, 125124 (2005).
[44] G. Bergmann, Phys. Rep. **107**, 1 (1984).
[45] E. McCann, K. Kechedzhi, V. I. Fal'ko, H. Suzuura, T. Ando, and B. L. Altshuler, Phys. Rev. Lett. **97**, 146805 (2006).
[46] I. L. Aleiner and K. B. Efetov, Phys. Rev. Lett. **97**, 236801 (2006).
[47] E. McCann and V. I. Fal'ko, Phys. Rev. Lett. **108**, 166606 (2012).
[48] V. I. Fal'ko, K. Kechedzhi, E. McCann, B. L. Altshuler, H. Suzuura, and T. Ando, Solid State Commun. **143**, 33 (2007).
[49] F. V. Tikhonenko, D. W. Horsell, R. V. Gorbachev, and A. K. Savchenko, Phys. Rev. Lett. **100**, 056802 (2008).

[50] N. J. G. Couto, D. Costanzo, S. Engels, D.-K. Ki, K. Watanabe, T. Taniguchi, C. Stampfer, F. Guinea, and A. F. Morpurgo, Phys. Rev. X **4**, 041019 (2014).
[51] P. A. Lee and T. V. Ramakrishnan, Rev. Mod. Phys. **57**, 287 (1985).
[52] B. L. Altshuler, A. G. Aronov, and D. E. Khmelnitsky, J. Phys. C **15**, 7367 (1982).
[53] K. S. Tikhonov, W. L. Z. Zhao, and A. M. Finkel'stein, Phys. Rev. Lett. **113**, 076601 (2014).
[54] X. Hong, K. Zou, B. Wang, S. H. Cheng, and J. Zhu, Phys. Rev. Lett. **108**, 226602 (2012).
[55] M. B. Lundeberg, R. Yang, J. Renard, and J. A. Folk, Phys. Rev. Lett. **110**, 156601 (2013).
[56] G. Bergmann, Phys. Rev. Lett. **48**, 1046 (1982).
[57] Z. Wang, D.-K. Ki, J. Y. Khoo, D. Mauro, H. Berger, L. S. Levitov, and A. F. Morpurgo, Phys. Rev. X **6**, 041020 (2016).
[58] A. Zangwill, *Physics at Surfaces* (Cambridge University Press, Cambridge, 1988).
[59] Y.-C. Lin, C. Jin, J.-C. Lee, S.-F. Jen, K. Suenaga, and P.-W. Chiu, ACS Nano **5**, 2362 (2011).
[60] Y.-C. Lin, C.-C. Lu, C.-H. Yeh, C. Jin, K. Suenaga, and P.-W. Chiu, Nano Lett. **12**, 414 (2012).